

Heterocyclic donor influences on the binding and activation of CO, NO, and O₂ by copper complexes of hybrid triazacyclononane–pyridyl ligands

Lisa M. Berreau, Jason A. Halfen, Victor G. Young Jr., William B. Tolman *

Department of Chemistry and the Center for Metals in Biocatalysis, 207 Pleasant St. S.E., Minneapolis, MN 55455, USA

Received 11 March 1999; accepted 11 June 1999

Dedicated to Professor Stephen J. Lippard on the occasion of his 60th birthday.

Abstract

Copper(I) complexes of 1,4-diisopropyl-7-R''-1,4,7-triazacyclononane (R'' = 2-pyridylmethyl, L^{Py}; 6-methyl-2-pyridylmethyl, L^{6MePy}; 5-methyl-2-pyridylmethyl, L^{5MePy}; 6-phenyl-2-pyridylmethyl, L^{6PhPy}; 2-quinolylmethyl, L^{Quin}) were prepared and characterized by CHN analysis, NMR and FTIR spectroscopy, cyclic voltammetry, and mass spectrometry. An X-ray crystal structure of [L^{6PhPy}Cu]SbF₆ was determined and compared to that previously reported for [L^{Py}Cu]O₃SCF₃; similar distorted trigonal bipyramidal geometries are adopted with the ligands coordinated in η⁴ fashion. The complexes [LCu]⁺ (L = L^{Py} or L^{Quin}) form adducts with CO(g) in which the heterocyclic appendage is displaced. With NO(g), [L^{Py}Cu]O₃SCF₃ reacts in a disproportionation process to yield N₂O and [L^{Py}Cu(ONO)]O₃SCF₃, which was structurally defined by X-ray crystallography. Upon reaction with O₂(g) at –75°C the Cu(I) complexes of L^{Py} and L^{5MePy} yield *trans*-1,2-peroxo species [LCuOOCuL]²⁺ as determined by UV–Vis and resonance Raman spectroscopy. In contrast, spectroscopy indicates that low temperature oxygenation of [L^{6PhPy}Cu]SbF₆ yields a bis(μ-oxo)dicopper core, postulated to be capped by η³-L^{6PhPy} (pyridyl appendage not coordinated). Decomposition of the *trans*-1,2-peroxo compounds results in hydroxylation of the ligand at the benzylic position of the heterocyclic appendage, but the bis(μ-oxo) complexes decay to give products resulting from N-dealkylation of the heterocycle arm. The different fates of the Cu(I) complexes of L^{Py} and L^{5MePy} versus that of L^{6PhPy} upon oxygenation may be traced to the coordination of the heterocycle; in the former cases, the pyridyl unit remains coordinated, favoring *trans*-1,2-peroxo generation, whereas pyridyl dissociation facilitated by the sterically bulky 6-phenyl group on L^{6PhPy} yields a [η³-L^{6PhPy}Cu]⁺ fragment amenable to bis(μ-oxo) core formation. The steric properties of the heterocyclic components of the ligands used in this study thus are important determinants of the reactivity of their Cu(I) complexes with small molecules. © 2000 Elsevier Science S.A. All rights reserved.

Keywords: Dioxygen activation; Vitric oxide; Copper complexes; Macrocylic complexes

1. Introduction

An important objective of bioinorganic chemistry research is to understand how small molecules such as carbon monoxide (CO), nitric oxide (NO), and dioxygen (O₂) bind to and/or are activated by metalloprotein active sites during catalytic processes [1], as signaling agents [2], or as probes of the active site's structure [3]. A successful strategy in synthetic investigations focused

on modeling the structural and functional aspects of the interactions of CO, NO, and O₂ with transition metal centers in biology is to use multidentate, chelating N-donor ligands to mimic the common ligation of such centers by multiple histidine imidazoles [4]. Implementation of this strategy to model copper active site chemistry recently has provided significant insights into the structures of Cu–CO, –O₂, and –NO adducts and pathways of NO and O₂ activation [5]. These studies have revealed that the supporting multidentate N-donor ligand plays a significant role in controlling the small molecule binding and activation chemistry, as

* Corresponding author. Tel.: +1-612-625 4061; fax: +1-612-624 7029.

E-mail address: tolman@chem.umn.edu (W.B. Tolman)

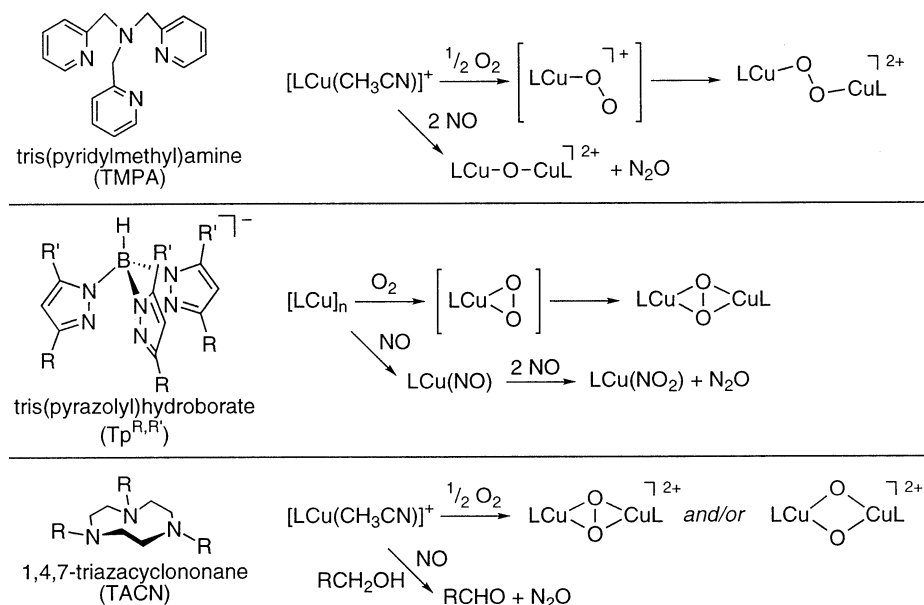


Fig. 1. Summary of reactions of O_2 and NO with copper(I) complexes supported by the indicated ligands.

illustrated by the complementary reactivities of copper(I) complexes of the tris(pyridylmethyl)amine (TPMA) [6], tris(pyrazol-1-yl)hydroborate ($\text{Tp}^{\text{R},\text{R}'}$) [7], and 1,4,7-triazacyclononane (TACN) ligand classes [8], among others¹ (Fig. 1).

For example, reaction of O_2 with $[(\text{TPMA})\text{Cu}(\text{CH}_3\text{CN})]^+$ at low temperature generates a (*trans*-1,2-peroxy)dicopper(II) complex [10] (Fig. 1). A monomeric (superoxo)copper intermediate is implicated in this reaction [11], and by using the derivative ligand bis(quinolylmethyl)(pyridylmethyl)amine (BQPA) this $\text{Cu}-\text{O}_2$ intermediate may be stabilized sufficiently to be observed via spectroscopy [12]². In contrast, oxygenation of copper(I) complexes of $\text{Tp}^{\text{R},\text{R}'}$ ($\text{R} = \text{R}' = \text{Me}$, ^iPr , or Ph) yields a (μ - η^2 : η^2 -peroxy)dicopper(II) species [14] analogous to the oxygenated active sites of hemocyanin, tyrosinase, and catechol oxidase [1d,15]. Involvement of a monocopper superoxo intermediate in this oxygenation is implicated by the isolation and X-ray structural determination of an analog supported by $\text{Tp}^{\text{Bu},\text{Pr}}$ that contains superoxide coordinated in η^2 (side-on) fashion [16]. The complexes $[(\text{R}_3\text{TACN})\text{Cu}(\text{CH}_3\text{CN})]^+$ also afford (μ - η^2 : η^2 -peroxy)dicopper species, but can yield

isomeric bis(μ -oxo)dicopper compounds as well, depending on the substituent R and other factors [1b]. Other important reactivity differences are exhibited in reactions with NO (Fig. 1). Thus, $[(\text{TPMA})\text{Cu}(\text{CH}_3\text{CN})]^+$ yields N_2O and a (μ -oxo)dicopper(II) complex [17], $\text{Tp}^{\text{R},\text{R}'}\text{Cu}(\text{CH}_3\text{CN})$ binds NO to give isolable adducts $\text{Tp}^{\text{R},\text{R}'}\text{Cu}(\text{NO})$ that react further to yield N_2O and copper(II)-nitrite species in a disproportionation process [18], and $[(^i\text{Pr}_3\text{TACN})\text{Cu}(\text{CH}_3\text{CN})]^+$ catalytically oxidizes alcohol solvent with concomitant generation of N_2O [19].

Factors that influence the course of the chemistry of copper(I) complexes of these TPMA, $\text{Tp}^{\text{R},\text{R}'}$, and TACN (as well as other) ligands include the number of N-donor atoms (3 for $\text{Tp}^{\text{R},\text{R}'}$ and TACN, 4 for TPMA), the nature of the N-donors (pyrazolyl for $\text{Tp}^{\text{R},\text{R}'}$, pyridyl and amine for TPMA, amine only for TACN), charge of the ligand (monoanionic for $\text{Tp}^{\text{R},\text{R}'}$, neutral for TPMA and TACN), and the size and electronic effects of ligand substituents that may or may not be oriented similarly with respect to the substrate binding site(s) on the copper ion. A goal of current research is to understand how such various, disparate, and often conflicting influences ‘tune’ small molecule binding and activation [20]. As part of our efforts aimed at addressing these issues, we have begun to investigate the structures and reactivities of copper complexes of ‘hybrid’ ligands that incorporate features of two or more of the aforementioned ligand classes. We report herein the results of studies of copper(I) complexes supported by one type of such a hybrid ligand comprising a single heterocyclic donor appended to 1,4-diisopropyl-1,4,7-triazacyclononane³ (Scheme 1). Our inves-

¹ Selected examples of related ligand types used in copper-small molecule chemistry include tris(imidazolyl)phosphine [9a–c], bis(pyridylmethyl)amine [9d–f], tris(pyrazolylethyl)amine [9g] and simple diamines [9h–j].

² An X-ray crystal structure of a monocopper superoxo complex of a derivative of TPMA with amide arms was reported [13a], but was shown to be incorrect [13b]. A paper reiterating the previous claims that this species exists in solution has appeared recently [13c], but in our view the interpretation of the newly provided supporting evidence remains ambiguous (cf. NMR data consistent with a small amount of uncomplexed ligand rather than the putative superoxo compound).

³ Similarly functionalized TACN (and other macrocyclic) ligands are surveyed in Ref. [21].

tigations of the structures, spectroscopic features, and reactivities with O₂, NO, and CO of copper(I) complexes of these ligands have revealed interesting similarities and differences with their TACN- and TMPA-coordinated counterparts, thus shedding new light on the general issue of ligand effects on copper ion-small molecule interactions in chemistry and biology. Portions of this work have been communicated [22,23].

2. Experimental

2.1. General procedures

All reagents and solvents were obtained from commercial sources and used as received unless noted otherwise. Solvents were dried according to standard procedures and distilled under N₂ immediately prior to use. Air-sensitive reactions were performed either in a Vacuum Atmospheres inert-atmosphere glovebox under a N₂ atmosphere or by using standard Schlenk and vacuum-line techniques. Methods used for physical characterization were as described previously [24]. Published procedures were used for the preparation of 1,4-diisopropyl-1,4,7-triazacyclononane (L^H) [23], 1,4-diisopropyl-7-(2-pyridylmethyl)-1,4,7-triazacyclononane (L^{Py}) [23], 2-chloromethyl-6-methylpyridine hydrochloride [25], 2-chloromethyl-5-methylpyridine hydrochloride [26], 2-chloromethyl-6-phenylpyridine [27], and [Cu(CH₃CN)₄]SbF₆ [28].

2.2. 1,4-Diisopropyl-7-(6-methyl-2-pyridylmethyl)-1,4,7-triazacyclononane (L^{6MePy})

To a solution of L^H (0.340 g, 1.60 mmol) in dry CH₃CN (20 ml) were added 2-chloromethyl-6-methylpyridine hydrochloride (0.284 g, 1.60 mmol), Na₂CO₃ (0.393 g), and n-Bu₄NBr (~ 5 mg). The result-

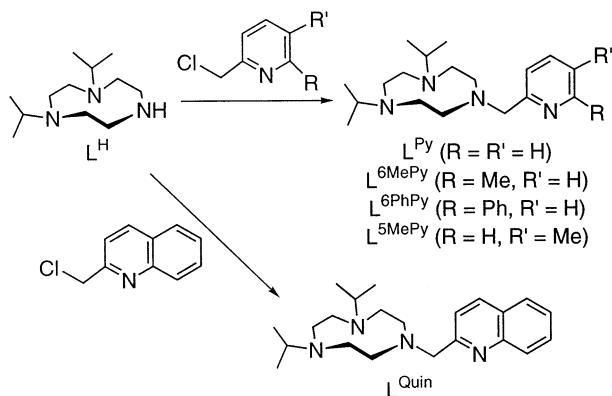
tant mixture was heated at reflux under N₂ for 14 h, after which time it was cooled to room temperature and then poured into 1 M NaOH (20 ml). The heterogeneous mixture was extracted with CHCl₃ (3 × 100 ml) and the organic extracts dried (Na₂SO₄) and filtered. Removal of the solvent under reduced pressure yielded a yellow-brown oil which was purified by Kugelrohr distillation (108–116°C, 0.1 torr) to afford the pure product as a clear, colorless oil (0.304 g, 60%). ¹H NMR (300 MHz, CDCl₃): δ 7.51 (t, *J* = 7.5 Hz, 1H), 7.41 (d, *J* = 7.5 Hz, 1H), 6.95 (d, *J* = 7.5 Hz, 1H), 3.80 (s, 2H), 2.93 (m, 4H), 2.90 (heptet, *J* = 6.6 Hz, 2H), 2.63 (m, 4H), 2.58 (s, 4H), 2.51 (s, 3H), 0.94 (d, *J* = 6.6 Hz, 12H) ppm; ¹³C{¹H} NMR (75 MHz, CDCl₃) δ 160.7, 157.2, 136.4, 120.9, 119.7, 64.0, 55.5, 54.8, 52.7, 52.5, 24.5, 18.4 ppm; FTIR (neat, cm⁻¹) 2962, 2823, 2899, 2871, 2802, 1677, 1591, 1580, 1456, 1380, 1359, 1306, 1261, 1169, 1115, 1092, 1034, 999, 973, 882, 851, 788, 769, 709, 568; high resolution electron impact mass spectrum (HREIMS) calc. for C₁₉H₃₄N₄: 318.2783; found: 318.2784.

2.3. 1,4-Diisopropyl-7-(5-methyl-2-pyridylmethyl)-1,4,7-triazacyclononane (L^{5MePy})

To a solution of L^H (0.386 g, 1.81 mmol) in dry CH₃CN (20 ml) were added 5-methyl-2-picolyl chloride hydrochloride (0.333 g, 1.87 mmol), Na₂CO₃ 90.400 g, 3.77 mmol), and n-Bu₄NBr (~ 3 mg). The resulting solution was heated at reflux under N₂ for 24 h. Following a work-up procedure identical to that outlined for L^{6MePy}, a yellow-brown oil was obtained which was purified by Kugelrohr distillation (102–110°C, 0.1 torr) to afford the product as a clear, colorless oil (0.347 g, 60%). ¹H NMR (300 MHz, CDCl₃): δ 8.33 (s, 1H), 7.45 (m, 2H), 3.80 (s, 2H), 2.97–2.93 (m, 4H), 2.87 (heptet, *J* = 6.6 Hz, 2H), 2.66–2.62 (m, 4H), 2.57 (s, 4H), 2.29 (s, 3H), 0.94 (d, *J* = 6.6 Hz, 12H) ppm; ¹³C{¹H} NMR (75 MHz, CDCl₃): δ 158.4, 149.1, 136.8, 130.8, 122.5, 63.4, 55.2, 54.8, 52.7, 52.5, 18.4, 18.1 ppm; FTIR (neat, cm⁻¹) 2966, 2933, 2903, 2821, 1674, 1599, 1569, 1487, 1459, 1380, 1359, 1312, 1263, 1170, 1150, 1114, 1093, 1032, 996, 973, 828, 735, 646, 581, 572, 561, 510, 497; HREIMS calc. for C₁₉H₃₄N₄: 318.2783; found: 318.2784.

2.4. 1,4-Diisopropyl-7-(6-phenyl-2-pyridylmethyl)-1,4,7-triazacyclononane (L^{6PhPy})

To a solution of L^H (0.331 g, 1.55 mmol) in dry CH₃CN (15 ml) were added 2-(chloromethyl)-6-phenylpyridine hydrochloride (0.372 g, 1.55 mmol), Na₂CO₃ (0.400 g, 3.77 mmol), and n-Bu₄NBr (~ 2 mg). The resulting solution was heated at reflux under N₂ for 6h. Following a basic work-up procedure identical to



Scheme 1.

that outlined for L^{6MePy}, the crude ligand was isolated as a yellow–orange oil. This oil was dissolved in methanol (3 ml) and the resulting pale yellow solution was added to a methanol/water (4:1 v/v, 5 ml) solution containing NaClO₄ (~0.4 g). To this solution was added excess water (5 ml) which led to the deposition of a viscous tan oil. This oil was then redissolved in CHCl₃ (~10 ml) and the resulting pale yellow organic solution was washed with 1 M NaOH (~10 ml). The organic phase was removed and the aqueous phase was extracted a second time with CHCl₃ (25 ml). The combined organic fractions were dried (Na₂SO₄) and the solvent was removed to yield the pure product as a thick, yellow oil (0.243 g, 41%). ¹H NMR (300 MHz, CDCl₃) δ 7.98 (d, *J* = 7.5 Hz, 2H), 7.71 (t, *J* = 7.8 Hz, 1H), 7.55 (d, *J* = 8.1 Hz, 2H), 7.46 (t, *J* = 6.9 Hz, 2H), 7.44 (t, *J* = 7.8 Hz, 1H), 3.94 (s, 2H), 2.94–3.02 (m, 4H), 2.91 (heptet, *J* = 6.6 Hz, 2H), 2.64–2.70 (m, 4H), 2.63 (s, 4H), 0.97 (d, *J* = 6.6 Hz, 12H) ppm; ¹³C{¹H} NMR (75 MHz, CDCl₃) δ 161.3, 156.4, 139.8, 136.9, 128.7, 126.9, 121.3, 118.4, 64.1, 55.7, 54.8, 52.8, 52.5, 18.4 (14 peaks observed out of 15 expected); FTIR (neat, cm⁻¹) 3066, 3034, 2963, 2935, 2895, 2857, 2817, 1575, 1454, 1380, 1358, 1309, 1259, 1165, 1112, 1091, 1033, 997, 917, 814, 758, 690, 669, 621, 573, 529; HREIMS calc. for C₂₄H₃₆N₄: 380.2940; found: 380.2941.

2.5. 1,4-Diisopropyl-7-(2-quinolylmethyl)-1,4,7-triazacyclononane (L^{Quin})

To a solution of L^H (0.326 g, 1.53 mmol) in CH₃CN (20 ml) were added 2-chloromethylquinoline hydrochloride (0.326 g, 1.52 mmol), Na₂CO₃ (0.400 g, 3.77 mmol), and tetrabutylammonium bromide (~5 mg). The resulting solution was heated at reflux for 12 h. Following a basic work-up procedure identical to that outlined for L^{6MePy}, the ligand was isolated as a red oil (0.536 g, 98%) of sufficient purity to be used without further manipulation. ¹H NMR (300 MHz, CDCl₃) δ 8.08 (d, *J* = 8.4 Hz, 1H), 8.03 (d, *J* = 8.4 Hz, 1H), 7.78 (d, *J* = 7.8 Hz, 1H), 7.76 (d, *J* = 7.8 Hz, 1H), 7.65 (dt, *J* = 1.2, 9.3 Hz, 1H), 7.47 (dt, *J* = 0.6, 7.2 Hz, 1H), 3.98 (s, 2H), 2.96 (m, 4H), 2.88 (heptet, *J* = 6.6 Hz, 2H), 2.64 (m, 4H), 2.59 (s, 4H), 0.94 (d, *J* = 6.6 Hz, 12H) ppm; ¹³C{¹H} NMR (75 MHz, CDCl₃) δ 162.2, 147.5, 136.0, 129.1, 128.9, 127.5, 127.7, 125.8, 121.4, 64.7, 55.6, 54.8, 52.7, 52.5, 18.4 ppm; HREIMS calc. for C₂₂H₃₄N₄: 354.2783; found: 354.2783.

2.6. [L^{6MePy}Cu]SbF₆

To a solution of L^{6MePy} (333 mg, 1.05 mmol) in CH₃CN/THF (2:1, 2 ml total volume) was added solid [Cu(CH₃CN)₄]SbF₆ (430 mg, 0.93 mmol). The mixture was stirred at room temperature until all of the Cu(I)

starting material had dissolved (~10 min). The resulting bright yellow solution was then added to Et₂O (15 ml) and was cooled to -20°C overnight, which led to the deposition of the product as a yellow microcrystalline solid (408 mg, 68%). ¹H NMR (300 MHz, d₆-acetone) δ 7.86 (t, *J* = 7.8 Hz, 1H), 7.45 (d, *J* = 7.8 Hz, 1H), 7.31 (d, *J* = 7.8 Hz, 1H), 4.27 (s, 2H), 3.30–2.78 (m, 14H), 2.78 (s, 3H), 1.28 (d, *J* = 6.6 Hz, 6H), 1.21 (d, *J* = 6.6 Hz, 6H) ppm; ¹³C{¹H} NMR (75 MHz, d₆-acetone) δ 158.5, 156.3, 137.6, 123.5, 121.1, 60.3, 57.9, 52.2, 51.5, 50.6, 27.2, 20.0 ppm; FTIR (KBr, cm⁻¹) 656 (SbF₆); UV-Vis (THF) [λ_{max}, nm (ε, M⁻¹ cm⁻¹)] 364 (3400); FAB-MS (MNBA) *m/e* (relative intensity) 381.2 ([M – SbF₆]⁺, 100%). *Anal. Calc.* for C₁₉H₃₄N₄CuSbF₆: C, 37.01; H, 5.56; N, 9.09. Found: C, 36.19; H, 5.38; N, 8.92%.

2.7. [L^{5MePy}Cu]SbF₆

To a solution of L^{5MePy} (308 mg, 0.97 mmol) in CH₃CN/THF (2:1, 2 ml total volume) was added solid [Cu(CH₃CN)₄]SbF₆ (430 mg, 0.93 mmol). The mixture was stirred at room temperature for ~10 min. The resulting dull orange solution was added to Et₂O (15 ml) and the solution was allowed to stand at ambient temperature for ~30 min during which time a thick, dark oil deposited. The remaining bright yellow solution was decanted away from the dark oil and was cooled to -20°C for 4 h, which led to the deposition of the product as a yellow microcrystalline solid (180 mg, 29%). ¹H NMR (300 MHz, d₆-acetone, 20°C) δ 7.77 (d, *J* = 7.8 Hz, 1H), 7.6 (br s, 2H), 3.2 (vbr s, 16H), 2.41 (s, 3H), 1.37 (d, *J* = 5.4 Hz, 6H), 1.24 (d, *J* = 5.3 Hz, 6H) ppm; FTIR (KBr, cm⁻¹) 2977, 2922, 1489, 1462, 1387, 1369, 1144, 1124, 1071, 952, 824, 656 (SbF₆); UV-Vis (THF) [λ_{max}, nm (ε, M⁻¹ cm⁻¹)] 364 (4900); FAB-MS *m/e* (relative intensity) 381.2 ([M – SbF₆]⁺, 100%). *Anal. Calc.* for C₁₉H₃₄N₄CuSbF₆: C, 37.01; H, 5.56; N, 9.09. Found: C, 36.95; H, 5.53; N, 9.08%.

2.8. [L^{6PhPy}Cu]SbF₆

To a solution of L^{6PhPy} (373 mg, 0.981 mmol) in CH₃CN/THF (2:1, 2 ml total volume) was added solid [Cu(CH₃CN)₄]SbF₆ (380 mg, 0.820 mmol). The mixture was stirred at room temperature for ~10 min and the resulting bright orange solution was added to Et₂O (15 ml). Cooling of the resulting solution overnight at -20°C led to the deposition of the orange microcrystalline product (390 mg, 70%). Crystals suitable for X-ray diffraction were obtained upon allowing a dilute solution of the complex in CH₃CN/Et₂O (~1:4) to stand at -20°C for 3–4 days. ¹H NMR (300 MHz, d₆-acetone) δ 8.09–8.00 (m, 3H), 7.78 (d, *J* = 7.8 Hz, 1H), 7.62–7.50 (m, 4H), 4.33 (s, 2H), 3.22–3.00 (m,

6H), 2.89–2.72 (m, 8H), 1.05 (d, $J = 6.6$ Hz, 6H), 0.97 (d, $J = 6.6$ Hz, 6H) ppm; $^{13}\text{C}\{^1\text{H}\}$ NMR (75 MHz, d_6 -acetone) δ 159.3, 157.3, 141.6, 138.2, 129.8, 129.0, 127.4, 123.4, 123.0, 60.4, 57.9, 51.8, 51.5, 50.5, 20.7, 18.6 ppm; FTIR (KBr, cm^{-1}) 659 (SbF_6^-); UV–Vis (THF) [λ_{max} , nm (ϵ , $\text{M}^{-1} \text{cm}^{-1}$)] 388 (2600); FAB-MS m/z (relative intensity) 443.2 ($[\text{M} - \text{SbF}_6]^+$, 100%). *Anal. Calc.* for $\text{C}_{24}\text{H}_{36}\text{N}_4\text{CuSbF}_6$: C, 42.47; H, 5.35; N, 8.26. Found: C, 42.25; H, 5.21; N, 8.26%.

2.9. $[\text{L}^{\text{Quin}}\text{Cu}]\text{SbF}_6$

A solution of L^{Quin} (0.071 g, 0.20 mmol) in EtCN (2 ml) was treated with solid $[\text{Cu}(\text{CH}_3\text{CN})]\text{SbF}_6$ (0.090 g, 0.19 mmol) producing a deep red solution. After stirring for 1 h, Et_2O (10 ml) was added which resulted in the precipitation of the product as red microcrystals. Further purification was accomplished by recrystallization from THF/ Et_2O (0.112 g, 86%). ^1H NMR (300 MHz, CD_3CN) δ 8.41 (d, $J = 8.4$ Hz, 1H), 8.26 (d, $J = 8.4$ Hz, 1H), 8.02 (d, $J = 7.8$ Hz, 1H), 7.86 (t, $J = 7.2$ Hz, 1H), 7.68 (t, $J = 7.2$ Hz, 1H), 7.49 (d, $J = 8.7$ Hz, 1H), 4.33 (s, 2H), 3.20–3.08 (m, 4H), 3.02–2.84 (m, 6H), 2.82–2.60 (m, 4H), 1.21 (d, $J = 6.6$ Hz, 6H), 1.16 (d, $J = 6.6$ Hz, 6H) ppm; $^{13}\text{C}\{^1\text{H}\}$ NMR (75 MHz, CDCl_3) δ 160.2, 145.2, 137.1, 130.5, 129.3, 128.5, 128.2, 127.4, 121.6, 62.2, 57.7, 53.0, 50.9, 50.5, 19.8 ppm; FTIR (KBr, cm^{-1}) 659 (SbF_6^-); UV–Vis (CH_2Cl_2) [λ_{max} , nm (ϵ , $\text{M}^{-1} \text{cm}^{-1}$)] 416 (4500); FAB-MS m/z (relative intensity) 417 ($[\text{M} - \text{SbF}_6]^+$, 100%). *Anal. Calc.* for $\text{C}_{22}\text{H}_{34}\text{N}_4\text{F}_6\text{CuSb}$: C, 40.42; H, 5.24; N, 8.57. Found: C, 40.74; H, 5.23; N, 8.72%.

2.10. Reaction of $[\text{L}^{\text{Py}}\text{Cu}]\text{CF}_3\text{SO}_3$ with $\text{NO}(\text{g})$

A solution of $[\text{L}^{\text{Py}}\text{Cu}]\text{CF}_3\text{SO}_3$ (0.250 g, 0.48 mmol) in THF/ CH_3CN (9:1, 10 ml) was exposed to 1 atm $\text{NO}(\text{g})$. After stirring for 30 min, excess $\text{NO}(\text{g})$ and the solvent were removed under vacuum. The blue–green residue was redissolved in THF, an equal volume of Et_2O was added, and the cloudy solution stored at -20°C overnight. The resultant blue crystalline mass was collected, washed with Et_2O , and dried under vacuum. Recrystallization from $\text{CH}_2\text{Cl}_2/\text{Et}_2\text{O}$ afforded blue crystals of $[\text{L}^{\text{Py}}\text{Cu}(\text{ONO})]\text{CF}_3\text{SO}_3 \cdot \text{CH}_2\text{Cl}_2$ suitable for X-ray crystallographic analysis (0.247 g, 79%). EPR (9.46 GHz, 77 K, 1:1 $\text{CH}_2\text{Cl}_2/\text{toluene}$) $g_z = 2.22$, $A_z = 150$ G, $g_y = 2.08$; $g_x = 2.00$; UV–Vis (THF) [λ_{max} , nm (ϵ , $\text{M}^{-1} \text{cm}^{-1}$)] 388 (590), 622 (150); FTIR (KBr, cm^{-1}) 1265 (CF_3SO_3^-), 1115 (CF_3SO_3^-), 1028 (CF_3SO_3^-), 637 (CF_3SO_3^-). *Anal. Calc.* for $\text{C}_{20}\text{H}_{34}\text{N}_5\text{O}_5\text{F}_3\text{SCl}_2\text{Cu}$: C, 37.07; H, 5.29; N, 10.81. Found: C, 37.69; H, 5.26; N, 10.81. Gaseous product analysis was performed as follows. A Schlenk flask of known volume (23.2 ml) was charged with a solution of $[\text{L}^{\text{Py}}\text{Cu}]\text{CF}_3\text{SO}_3$ (0.050 g, 0.097 mmol) in THF (2.00 ml) under N_2 . A single drop

Table 1
Spectroscopic properties of copper–dioxygen complexes

Complex	UV–Vis ^a λ_{max} (nm) (ϵ ($\text{M}^{-1} \text{cm}^{-1}$))	Resonance Raman ^b (cm^{-1})
$[\text{L}^{\text{Py}}\text{Cu}]_2(\text{O}_2)(\text{CF}_3\text{SO}_3)_2$	550 (10 200), 600 (9700)	822 (771), 530 (506)
$[\text{L}^{6\text{PhPy}}\text{Cu}]_2(\mu\text{-O})_2(\text{SbF}_6)_2$	316 (10 000), 432 (12 000)	584 (557)
$[\text{L}^{5\text{MePy}}\text{Cu}]_2(\text{O}_2)(\text{SbF}_6)_2$	550 (11 500), 594 (11 000)	823 (772), 530 (502), 476 (457)

^a Measured in either THF: CH_3CN (10:1, L^{Py}) or THF ($\text{L}^{6\text{PhPy}}$, $\text{L}^{5\text{MePy}}$) below -70°C .

^b The resonance Raman spectra were obtained at 77 K as frozen THF: CH_3CN (10:1, L^{Py}) or THF ($\text{L}^{6\text{PhPy}}$, $\text{L}^{5\text{MePy}}$) solutions using either 572 nm (L^{Py} and $\text{L}^{5\text{MePy}}$) or 457 nm ($\text{L}^{6\text{PhPy}}$) laser excitation; only ^{18}O sensitive vibrations are given with specific ^{18}O shifts indicated in parentheses.

of CH_3CN was added to clarify the solution. The headspace was then rapidly replaced with NO and the reaction stirred vigorously under NO with occasional shaking for 24 h. The headspace was then sampled with a gas-tight syringe; GC analysis (HP 5180 GC; 6 m Propak-Q column; flow rate = 20 ml min^{-1} ; temp. = 30°C) of the headspace gas revealed the presence of N_2O (retention time 4.0 min; yield = 63% based on $[\text{L}^{\text{Py}}\text{Cu}]^+$, average of three replicate runs).

2.11. Reversible reactions of $[\text{L}^{\text{P}}\text{Cu}]\text{SbF}_6$ ($\text{P} = \text{Py}$ or Quin) with $\text{CO}(\text{g})$

A solution of $[\text{L}^{\text{P}}\text{Cu}]\text{SbF}_6$ in THF (ca. 0.6 mM) was purged with $\text{CO}(\text{g})$ causing a rapid bleaching of the yellow–orange color (cf. UV–Vis spectra in Fig. S2). Analysis of aliquots by FTIR spectroscopy revealed $\nu_{\text{CO}} = 2067$ (L^{Py}), 2076 (L^{Quin}) cm^{-1} . The colorless solution was then purged with N_2 for 5 min, regenerating the original color and optical spectrum of $[\text{L}^{\text{P}}\text{Cu}]\text{X}$ (Fig. S2). This CO/N_2 protocol was repeated several times without appreciable decomposition.

2.12. Reactions of $[\text{L}^{\text{P}}\text{Cu}]\text{SbF}_6$ with $\text{O}_2(\text{g})$

Solutions of $[\text{L}^{\text{P}}\text{Cu}]\text{SbF}_6$ in THF (~ 0.5 – 20 mM) were cooled to about -75°C and exposed to dry O_2 which resulted in immediate color changes as described in the text. Samples for UV–Vis spectroscopy were prepared in a quartz UV–Vis cuvette modified for use at low temperature. Samples for EPR (0.5–2.0 mM) and resonance Raman (~ 20 mM) spectroscopies were prepared by removing aliquots of the solution with a pre-cooled (liq. N_2) pipette. Data are listed in Table 1.

In experiments aimed at identifying the decomposition products of the oxygenated species, the solutions

(~ 0.1 mM) were purged with $N_2(g)$ for 10 min after oxygenation was complete (UV–Vis) and then allowed to warm to room temperature. The resulting green solution was treated with aqueous NH_4OH (1 ml) and $CHCl_3$ (5 ml) with vigorous stirring. The organic phase was then removed, and the blue aqueous phase extracted with $CHCl_3$ (2×10 ml). The combined organic extracts were dried (Na_2SO_4) and evaporated to yield a yellow residue (mass recovery: L^{6MePy} , 93%; L^{6PhPy} , 88%; L^{Quin} , 88%; L^{5MePy} , 61%) which was analyzed by 1H NMR spectroscopy and GC/MS. For $P = Py$ or $5MePy$, the presence of L^{5MePy} and L^{5MePyO} in an approximately 2:1 ratio was determined from 1H NMR spectra. For $P = 6MePy$, $6PhPy$, or $Quin$, L^P and L^H were identified in an approximately 3:2 ratio. The corresponding 2-carboxaldehyde coproduct in each of these N-dealkylation reactions was identified by 1H NMR and GC-MS but was present only in low yield ($< 20\%$ of expected amount based on yield of L^H) presumably due to decomposition under the conditions of the work-up procedure.

2.13. X-ray crystallography

Crystals of $[L^{6PhPy}Cu]SbF_6$ (orange block) and $[L^{Py}Cu(ONO)]CF_3SO_3 \cdot CH_2Cl_2$ (blue plate) were attached to a glass fiber with heavy-weight oil and mounted on a Siemens SMART CCD system for data collection at 173(2) K. Initial sets of cell constants were calculated from 70 or 137 strong reflections, respectively, harvested from three sets of 20 frames. Final cell constants were calculated from a set of 8192 or 5195 strong reflections from the data collection. The space groups $P2_1/n$ or $P\bar{1}$, respectively, were determined on the basis of systematic absences and intensity statistics. Successful direct-methods solutions were calculated which provided most of the non-hydrogen atoms from the E-map. Several full-matrix least-squares/difference Fourier cycles were performed which located the remainder of the non-hydrogen atoms. All non-hydrogen atoms were refined with anisotropic displacement parameters. All hydrogen atoms were placed in ideal positions and were refined as riding atoms with relative isotropic displacement parameters. Calculations were performed using SHELXTL-PLUS Version 5.0 [29]. Crystal data and refinement parameters are listed in Table 2 and selected bond distances and angles are shown in Table 3; full reports are provided as supporting information.

3. Results and discussion

3.1. Synthesis and spectroscopic characterization of ligands and copper(I) complexes

We prepared a series of ligands (Scheme 1) that differ with respect to the nature of the heterocyclic donor

(pyridyl or quinolyl) or the type and position (5- or 6-methyl; 6-phenyl) of pyridyl ring substituents. These new ligands were prepared via treatment of 1,4-diisopropyl-1,4,7-triazacyclononane (L^H) [22] with the appropriate 2-halomethyl-pyridyl or -quinolyl derivative and were isolated in ~ 40 – 60% yield following purification. All ligands were characterized by NMR spectroscopy and high resolution mass spectrometry.

Copper(I) complexes (Fig. 2) of L^P [$P = Py$, $6MePy$, $5MePy$, $6PhPy$, $Quin$] were prepared by treating the ligands with $[Cu(CH_3CN)_4]X$ ($X = SbF_6^-$ or $CF_3SO_3^-$) in CH_3CN or CH_3CN/THF (2:1) under an inert atmosphere. The complexes were isolated as yellow to orange–red air-sensitive microcrystalline solids and were characterized by CHN analysis, 1H and ^{13}C NMR and FTIR spectroscopy, fast atom bombardment mass spectrometry, and, in several cases, X-ray crystallography. Binding of the respective appended heterocyclic donor to Cu(I) in the complexes was evident from their UV–Vis spectra, which contained an intense (ϵ 3400–4500 $M^{-1} cm^{-1}$) band with $\lambda_{max} \cong 360$ (L^{Py} , L^{6MePy} , L^{5MePy}), 388 (L^{6PhPy}), or 420 nm (L^{Quin}) that may be

Table 2
X-ray crystallographic data ^a

	$[L^{6PhPy}Cu]SbF_6$	$[L^{Py}Cu(ONO)]O_3SCF_3 \cdot CH_2Cl_2$
Empirical formula	$C_{24}H_{36}N_4F_6SbCu$	$C_{20}H_{34}N_5O_5Cl_2F_3SCu$
Formula weight	679.86	646.10
Crystal system	monoclinic	triclinic
Space group	$P2_1/n$	$P\bar{1}$
<i>a</i> (Å)	18.4464(4)	9.8889(2)
<i>b</i> (Å)	9.6457(2)	12.7742(1)
<i>c</i> (Å)	16.0169(2)	13.2909(1)
α (°)	90	113.534(1)
β (°)	108.093(1)	93.394(1)
γ (°)	90	109.382(1)
<i>V</i> (Å ³)	2708.95(6)	1415.93(3)
<i>Z</i>	4	2
Density (calc.) ($g cm^{-3}$)	1.667	1.520
Temperature (K)	173(2)	173(2)
Crystal size (mm)	$0.18 \times 0.15 \times 0.12$	$0.50 \times 0.50 \times 0.25$
Diffractometer	Siemens SMART	Siemens SMART
Absorption coefficient (mm^{-1})	1.844	1.092
2θ max (°)	50.04	50.06
Reflections collected	13275	7105
Independent reflections	4748	4786
Variable parameters	331	372
R_1/wR_2 ^b	0.0314/0.0658	0.0430/0.1033
Goodness-of-fit (F^2)	1.036	1.062
Largest difference peak ($e \text{ \AA}^{-3}$)	0.646/−0.533	1.184/−0.757

^a Radiation used: Mo $K\alpha$ ($\lambda = 0.71073$ Å).

^b $R_1 = \sum ||F_o| - |F_c|| / \sum |F_o|$; $wR_2 = [\sum [w(F_o^2 - F_c^2)^2] / \sum w(F_o^2)^2]^{1/2}$ where $w = 1/\sigma^2(F_o^2) + (aP)^2 + bP$.

Table 3
Selected bond lengths (Å) and angles (°) for complexes characterized by X-ray crystallography^a

$[L^{Py}Cu]O_3SCF_3^b$			
Cu(1)–N(1)	2.167(3)	Cu(1)–N(2)	2.133(3)
Cu(1)–N(3)	2.108(3)	Cu(1)–N(5)	1.941(3)
N(1)–Cu(1)–N(2)	85.75(11)	N(1)–Cu(1)–N(3)	84.64(11)
N(1)–Cu(1)–N(4)	86.21(12)	N(2)–Cu(1)–N(3)	87.27(11)
N(3)–Cu(1)–N(4)	139.67(12)	N(2)–Cu(1)–N(4)	131.05(12)
$[L^{6PhPy}Cu]SbF_6$			
Cu(1)–N(1)	2.191(3)	Cu(1)–N(2)	2.070(3)
Cu(1)–N(3)	2.129(3)	Cu(1)–N(4)	1.948(3)
N(1)–Cu(1)–N(2)	84.85(11)	N(1)–Cu(1)–N(3)	84.30(11)
N(1)–Cu(1)–N(4)	84.60(11)	N(2)–Cu(1)–N(3)	88.28(11)
N(3)–Cu(1)–N(4)	122.77(11)	N(2)–Cu(1)–N(4)	145.83(11)
$[L^{Py}Cu(ONO)]O_3SCF_3 \cdot CH_2Cl_2$			
Cu(1)–N(1)	2.050(2)	Cu(1)–N(4)	2.061(2)
Cu(1)–N(7)	2.292(2)	Cu(1)–N(16)	2.001(2)
Cu(1)–O(1)	1.982(1)	O(1)–N(1A)	1.297(4)
N(1A)–O(2)	1.219(4)		
N(1)–Cu(1)–N(4)	168.24(9)	N(1)–Cu(1)–N(7)	84.09(9)
N(1)–Cu(1)–N(16)	82.65(10)	N(1)–Cu(1)–O(1)	168.4(9)
N(4)–Cu(1)–N(7)	85.49(9)	N(4)–Cu(1)–N(16)	168.04(10)
N(4)–Cu(1)–O(1)	96.43(10)	N(7)–Cu(1)–N(16)	96.03(10)
N(7)–Cu(1)–O(1)	107.57(9)	N(16)–Cu(1)–O(1)	94.42(10)

^a Estimated standard deviations indicated in parentheses.

^b Selected bond distances and angles for one independent cation (of two) in the asymmetric unit of $[L^{Py}Cu]O_3SCF_3$; X-ray crystallographic data for this complex has been previously reported, but metrical information is reproduced here for comparative purposes [22].

attributed to a Cu(I) → heterocycle MLCT transition [30]. The 1H NMR spectra of $[L^{Py}Cu]X$ ($X = O_3SCF_3^-$ or SbF_6^-) and $[L^{5MePy}Cu]SbF_6$ in CD_3CN or acetone- d_6 at or above ambient temperature (data acquired up to +55°C) contain sharp peaks for the iPr groups and 4-pyridyl hydrogen, but the remaining resonances are broad (cf. Fig. S1 in Supplementary material). Sharpening of the spectrum of $[L^{Py}Cu]SbF_6$ occurs as the temperature is lowered (data acquired to –85°C). These observations imply the existence of fluxionality in solution, perhaps involving binding and release of solvent, the pyridyl arm, or both. In contrast, 1H NMR

spectra at ambient temperature of $[L^{6PhPy}Cu]SbF_6$, $[L^{6MePy}Cu]SbF_6$, and $[L^{Quin}Cu]SbF_6$ exhibit sharp peaks consistent with retention of the structures determined by X-ray crystallography (vide infra) that exhibit η^4 -coordination of their respective supporting ligands. We

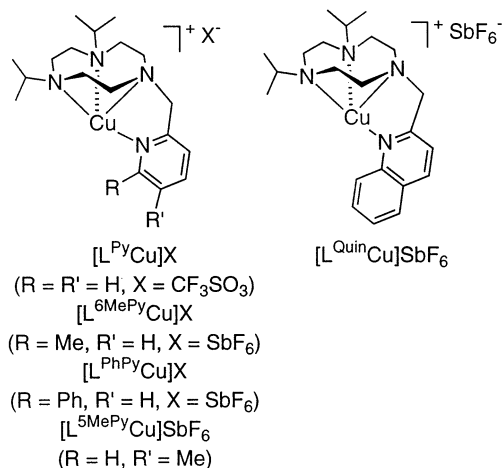


Fig. 2. Copper(I) complexes prepared in this study.

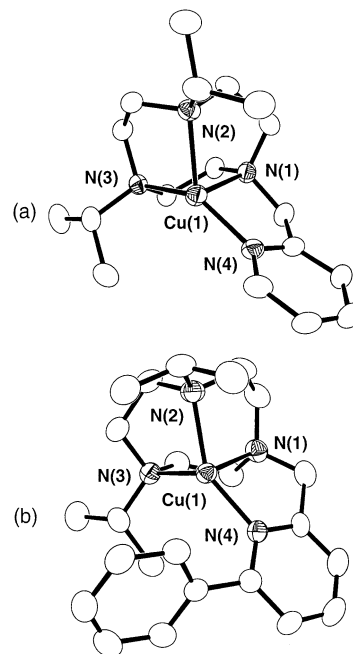


Fig. 3. Cationic portions of the X-ray crystal structures of (a) $[L^{Py}Cu]O_3SCF_3$ [22] and (b) $[L^{6PhPy}Cu]SbF_6$ showing non-hydrogen atoms as 50% ellipsoids.

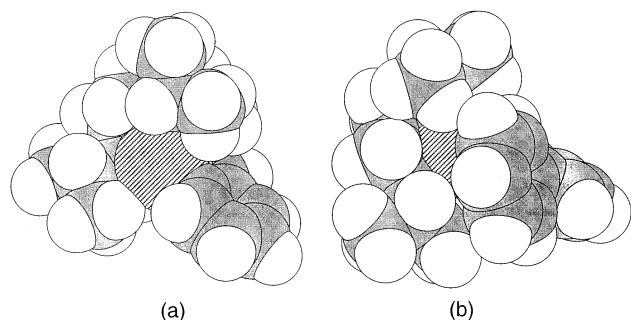


Fig. 4. Space-filling representations of the cationic portions of the X-ray crystal structures of (a) $[L^{\text{Py}}\text{Cu}]\text{O}_3\text{SCF}_3$ [22] and (b) $[L^{6\text{PhPy}}\text{Cu}]\text{SbF}_6$.

surmise that the absence of fluxional behavior for these complexes is due to the increased steric bulk of their heterocyclic appendages that makes the metal ion less accessible to solvent.

3.2. X-ray structures of copper(I) complexes

Drawings of the X-ray structures of the cationic portions of $[L^{\text{Py}}\text{Cu}]\text{O}_3\text{SCF}_3$ (communicated previously [22a] but shown here for comparative purposes; only one of two crystallographically independent but chemically similar molecules in the asymmetric unit is reproduced) and $[L^{6\text{PhPy}}\text{Cu}]\text{SbF}_6$ are presented in Fig. 3. Crystallographic data for the latter structure and selected bond distances and angles for both are listed in Tables 2 and 3, respectively. A preliminary X-ray crystal structure of $[L^{\text{Quin}}\text{Cu}]\text{SbF}_6$ indicated a topology closely analogous to those of the compounds coordinated by L^{Py} and $L^{6\text{PhPy}}$, but problems with pseudosymmetry and disorder prohibit a full description.

In $[L^{\text{Py}}\text{Cu}]\text{SbF}_6$ and $[L^{6\text{PhPy}}\text{Cu}]\text{SbF}_6$, two amine nitrogens and the heterocyclic nitrogen form the basal plane of a distorted trigonal pyramidal coordination geometry, with the third amine nitrogen (N1) occupying the axial position. The intraligand N–Cu–N bond angles within the basal plane in both structures are significantly distorted from the idealized value of 120° (L^{Py} , $\text{N}(2)\text{--Cu}(1)\text{--N}(3) = 87.3(1)^\circ$ and $\text{N}(3)\text{--Cu}(1)\text{--N}(4) = 139.7(1)^\circ$; $L^{6\text{PhPy}}$, $\text{N}(2)\text{--Cu}(1)\text{--N}(3) = 88.3(1)^\circ$ and $\text{N}(2)\text{--Cu}(1)\text{--N}(4) = 145.83(11)^\circ$), apparently as a result of the constrained nature of the triazamacrocyclic ring. Bond angles between the basal ligands and the axial N-donor N(1) are slightly acute (L^{Py} , avg. 85.4° ; $L^{6\text{PhPy}}$ avg. 84.6°), a consequence of a displacement of the copper ion slightly ($\sim 0.15 \text{ \AA}$) below the basal plane. In both structures, the Cu–N_{pyridyl} bond length (L^{Py} , $1.941(3) \text{ \AA}$; $L^{6\text{PhPy}}$ $1.948(3) \text{ \AA}$, respectively) is shorter than the other Cu–N bond lengths ($2.07\text{--}2.21 \text{ \AA}$), possibly reflecting increased Cu–N_{pyridyl} bond order arising from π -backdonation ($\text{Cu}(\text{I})d \rightarrow \text{heterocycle } \pi^*$).

Overall, the coordination geometries in both compounds are similar, the only significant difference between them being the degree of steric hindrance about a potential fifth coordination site (cf. space-filling drawings shown in Fig. 4). In $[L^{\text{Py}}\text{Cu}]^+$ this site lies within a pocket formed by the isopropyl substituents and the pyridyl donor and appears relatively accessible, whereas in $[L^{6\text{PhPy}}\text{Cu}]^+$ it is blocked by the phenyl substituent⁴. An intermediate degree of shielding of this site in $[L^{\text{Quin}}\text{Cu}]^+$ is apparent from the preliminary X-ray structural data and from molecular models. As described below, these differences in metal ion accessibility are of critical importance in small molecule reactivity studies.

For purposes of comparison to the structures of $[L^{\text{Py}}\text{Cu}]^+$ and $[L^{6\text{PhPy}}\text{Cu}]^+$, reproductions of the previously reported X-ray structures of Cu(I) complexes of related tetradentate tripodal ligands bis(pyridylmethyl)(6-carbomethoxy-pyridylmethyl)amine (TMPA') [10], tris(quinolylmethyl)amine (TMQA) [12], and tris(6-phenyl-pyridylmethyl)amine (TPPA) [27] are shown in Fig. 5. Of the five structures illustrated in Figs. 3–5, that of $[(\text{TMPA}')\text{Cu}(\text{CH}_3\text{CN})]^+$ is distinguished by the fact that it adopts a five-coordinate geometry with a bound acetonitrile ($\text{Cu}\text{--N}_{\text{CH}_3\text{CN}} = 1.999(9) \text{ \AA}$) *trans* to a weakly-ligated amine donor ($\text{Cu}\text{--N}_{\text{amine}} = 2.439(8) \text{ \AA}$). In contrast, the remaining four structures comprising more sterically hindered supporting ligands are qualitatively alike insofar as they adopt four-coordinate, approximately trigonal pyramidal geometries with no binding of exogenous acetonitrile. Closer inspection, however, reveals interesting differences between the topologies imposed by L^{Py} and $L^{6\text{PhPy}}$ compared to those of the hindered variants of TMPA. The Cu–N_{heterocycle} bond lengths in $[L^{\text{Py}}\text{Cu}]\text{SbF}_6$ ($1.941(3) \text{ \AA}$) and $[L^{6\text{PhPy}}\text{Cu}]\text{SbF}_6$ ($1.948(3) \text{ \AA}$) are shorter than the corresponding distances in $[(\text{TMQA})\text{Cu}]^+$ and $[(\text{TPPA})\text{Cu}]^+$ (avg. 2.01 and 2.12 \AA). In addition, in $[L^{\text{Py}}\text{Cu}]^+$ and $[L^{6\text{PhPy}}\text{Cu}]^+$ intraligand N–Cu–N bond angles within the basal plane are significantly distorted from 120° , but more regular angles are adopted in $[(\text{TMQA})\text{Cu}]^+$ ($122.1(2)$, $120.6(2)$ and $113.0(2)^\circ$) and $[(\text{TPPA})\text{Cu}]^+$ ($122.0(3)$, $119.0(3)$ and $112.2(3)^\circ$). This difference may be attributed to the less constrained nature of the TMQA and TPPA tripods compared to the L^{P} ligands, which have three out of the four potential donors fettered by the TACN macrocycle.

3.3. Electrochemistry

The half-wave potentials for all Cu(I) complexes were measured by cyclic voltammetry under a N_2 atmo-

⁴ Bonding interactions between the Cu(I) ion and the phenyl ring carbons in $[L^{6\text{PhPy}}\text{Cu}]^+$ appear to be absent on the basis of Cu–C distances $> 3 \text{ \AA}$.

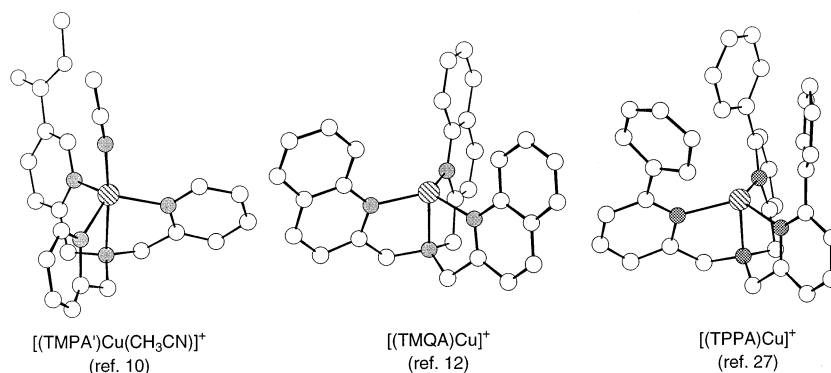


Fig. 5. Reproductions of the X-ray crystal structures of previously reported copper(I) complexes of TMPA derivatives.

sphere in CH_3CN solution with 0.1 M $(\text{Bu}_4\text{N})(\text{PF}_6)$ (Table 4, reported vs. SCE, Pt electrode). All of the complexes $[\text{L}^{\text{P}}\text{Cu}]\text{X}$ ($\text{R} = \text{Py}$, 6MePy, 5MePy, 6PhPy, Quin) exhibited a quasi-reversible, one-electron redox transformation with peak separations (ΔE_{p}) of ~ 90 – 110 mV at a scan rate of 0.02 V s^{-1} . Under identical experimental conditions, the ferrocene/ferrocenium couple was observed at 0.39 V versus SCE ($\Delta E_{\text{p}} (0.02 \text{ V s}^{-1}) = 100 \text{ mV}$).

The data listed in Table 4 indicate that the heterocyclic appendages have important effects on the Cu(I)/Cu(II) redox potential. Overall, the $E_{1/2}$ values for the new complexes are sufficiently low to favor participation of the Cu(I) compounds in O_2 activation chemistry. The potentials are lower than that measured previously for $[(\text{Pr}_3\text{TACN})\text{Cu}(\text{CH}_3\text{CN})]^+$ [24], which may be attributed — at least in part — to stabilization of the Cu(I) state in the latter by coordinated CH_3CN , a ‘softer’ donor that favors the cuprous state more than the heterocyclic appendages on L^{P} . The $[\text{L}^{\text{P}}\text{Cu}]^+$ complexes may be divided into two sets on the basis of their redox behavior; those with $E_{1/2} < 0 \text{ V}$ versus SCE ($\text{R} = \text{Py}$ and 5MePy) versus those with $E_{1/2} > 0 \text{ V}$ ($\text{R} = \text{Quin}$, 6MePy, and 6PhPy). Our analysis of how the nature of the heterocyclic donor group causes the ~ 0.2 – 0.3 V difference in redox potentials between these two sets of complexes follows those used by Karlin and co-workers [12], Canary and co-workers [27], and Sorrell and Jameson [9g] to rationalize data acquired for complexes of tetradentate tripodal TMPA, BQPA, TPPA, and related ligands (data listed in Table 4 for selected cases measured in CH_3CN).

The factors which have been shown to influence the redox potentials of copper complexes include: (1) type of donor atoms; (2) coordination geometry, and (3) ligand substituent effects. Differences in the basicity of the heterocyclic donor groups in the L^{P} chelates seem to have little effect on the position of the Cu(I)/Cu(II) redox couple. For example, the Cu(I) complex supported by $\text{L}^{6\text{MePy}}$ is oxidized at an identical potential to that supported by L^{Quin} despite significant differences in the

basicities of the two heterocyclic donor groups ($\text{p}K_{\text{b}} = 7.94$ and 9.12 , respectively) [31]. On the basis of the available solid state structural data that indicate homologous coordination topologies for $[\text{L}^{\text{Py}}\text{Cu}]\text{O}_3\text{SCF}_3$, $[\text{L}^{\text{Quin}}\text{Cu}]\text{SbF}_6$, and $[\text{L}^{6\text{PhPy}}\text{Cu}]\text{SbF}_6$ (vide supra), coordination geometry effects also would appear to be precluded as a rationale for the divergent $E_{1/2}$ values for the two sets of $[\text{L}^{\text{P}}\text{Cu}]^+$ complexes. On the other hand, the NMR data indicate that the Cu(I) complexes of L^{Py} and $\text{L}^{5\text{MePy}}$ (which have low redox potentials) are fluxional in solution, possibly due to equilibria involving solvent binding and release. While coordination of CH_3CN to the Cu(I) complexes of these ligands would be expected to raise rather than lower their redox potentials, solvent binding to the Cu(II) forms to yield stable five-coordinate geometries might explain their low $E_{1/2}$ values. Such solvent coordination, to either the Cu(I) or Cu(II) forms, would be inhibited sterically in the $\text{L}^{6\text{MePy}}$, $\text{L}^{6\text{PhPy}}$, and L^{Quin} cases (as borne out by the NMR spectral results, vide supra), resulting in higher redox potentials for these complexes. In addition to this direct ‘blocking’ effect of the ligand substituents that inhibits solvent coordination, a less specific shielding of the redox center from polar solvent by the hydrophobic appendages also may

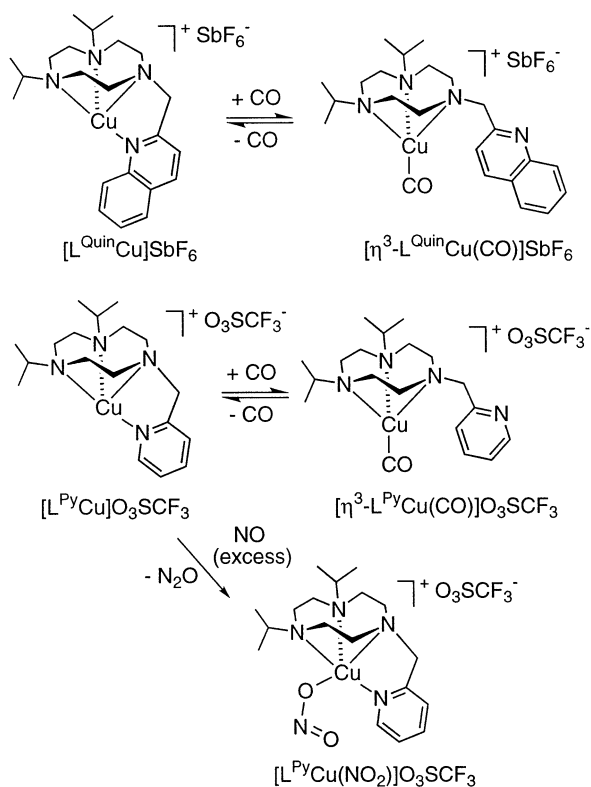
Table 4
Cyclic voltammetry data for Cu(I) complexes in CH_3CN vs. SCE ^a

Complex	$E_{1/2}$ (V)	ΔE_{p} (mV)	Ref.
$[\text{L}^{\text{Py}}\text{Cu}]^+$	−0.07	94	this work
$[\text{L}^{5\text{MePy}}\text{Cu}]^+$	−0.10	110	this work
$[\text{L}^{\text{Quin}}\text{Cu}]^+$	0.12	104	this work
$[\text{L}^{6\text{MePy}}\text{Cu}]^+$	0.13	102	this work
$[\text{L}^{6\text{PhPy}}\text{Cu}]^+$	0.26	92	this work
$[(\text{Pr}_3\text{TACN})\text{Cu}(\text{CH}_3\text{CN})]^+$	0.36	110	[24]
$[(\text{TPPA})\text{Cu}(\text{CH}_3\text{CN})]^+$	0.06	^b	[27]
$[(\text{TMPA})\text{Cu}(\text{CH}_3\text{CN})]^+$	−0.24	^c	[12]

^a For measurements made in this work, 0.1 M $(\text{Bu}_4\text{N})(\text{PF}_6)$ was used with a Pt electrode at 20°C .

^b Not reported for this solvent, but in DMF $\Delta E_{\text{p}} = 120 \text{ mV}$.

^c Not reported for this solvent, but in DMF $\Delta E_{\text{p}} = 78 \text{ mV}$.



contribute to the destabilization of the Cu(II) state and thus to the observation of high potentials for $[L^{6PhPy}Cu]^+$, $[L^{Quin}Cu]^+$, and $[L^{6MePy}Cu]^+$. Analogous arguments invoking increased hydrophobicity and/or solvent 'blocking' effects of the quinolyl and phenylpyridyl substituents of TMQA and TPPA relative to TMPA and of the methyl groups in the 3,5-dimethylpyrazolyl analog of tris[2-(1-pyrazolyl)ethyl]amine [9g] have been offered to explain the observed $E_{1/2}$ values for copper complexes of these ligands.

3.4. Reactivity of copper(I) complexes with small molecules

Because the principal focus of our studies has been to characterize ligand structural influences on dioxygen binding and activation by copper complexes, O_2 reactions with the entire set of $[L^P Cu]X$ compounds were examined. First, however, we describe the interactions of selected members of the set with CO and NO that illustrate key patterns of reactivity arising from specific features of the L^R ligand type.

3.4.1. Carbon monoxide

Treatment of $[L^P Cu]X$ ($P = \text{Quin}$, $X = \text{SbF}_6^-$; $P = \text{Py}$, $X = \text{O}_3\text{SCF}_3^-$) with CO results in bleaching of the color of the solution and growth of a ν_{CO} at 2076 or 2067

cm^{-1} , respectively (Scheme 2 and Fig. S2 in Supplementary material). The loss of the Cu(I) \rightarrow heterocycle MLCT feature upon binding of CO to $[L^P Cu]^+$ attests to displacement of the heterocyclic arm to yield four-coordinate adducts $[(\eta^3-L^P)Cu(CO)]SbF_6^-$. Purging of the colorless solutions of these adducts with N_2 for several minutes resulted in complete restoration of the original color and charge transfer intensity, indicating that CO binding and concomitant displacement of the heterocyclic arm are reversible. An analogous displacement of a pendant pyridyl donor by an exogenous ligand was observed in the reaction of $[(\text{TMPA})Cu(\text{CH}_3\text{CN})]^+$ with PPh_3 , yielding $[(\eta^3\text{-TMPA})Cu(\text{PPh}_3)]^+$ that was structurally characterized by X-ray crystallography [10]. Whether CO reacts with $[(\text{TMPA})Cu(\text{CH}_3\text{CN})]^+$ similarly or simply displaces CH_3CN is not firmly established. The CO adducts $[(R_3\text{TACN})Cu(CO)]^+$ exhibit similar ν_{CO} values to those supported by $\eta^3\text{-L}^P$, but due to the lack of a fourth potential donor do not lose CO and revert to their respective precursor complex nearly as readily [32]. In sum, the additional pyridyl or quinolyl donor group on the 1,4,7-triazacyclononane macrocyclic ligand framework in Cu(I) complexes is substituted by exogenous CO, but CO binding is rendered reversible by the facility with which the appended donor may rebound to the metal ion.

3.4.2. Nitric oxide

Exposure of THF/ CH_3CN (4:1) solutions of $[L^P Cu]CF_3SO_3$ to NO at room temperature resulted in a gradual color change from yellow to blue–green and the evolution of N_2O (yield = 65% by GC analysis of the headspace gas after 24 h). Removal of solvent followed by recrystallization afforded a single copper-containing compound, identified as the nitrito complex $[L^P Cu(\text{NO}_2)]CF_3SO_3$ (Scheme 2). The solid state structure of the complex as determined by X-ray crystallography is depicted in Fig. 6; crystallographic data and selected bond lengths and angles are presented in Tables 2 and 3, respectively. The central Cu(II) ion is

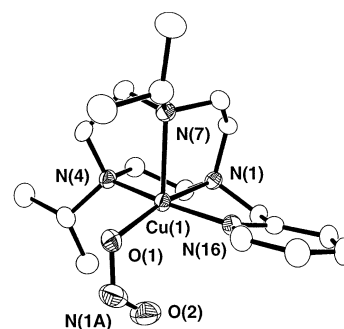
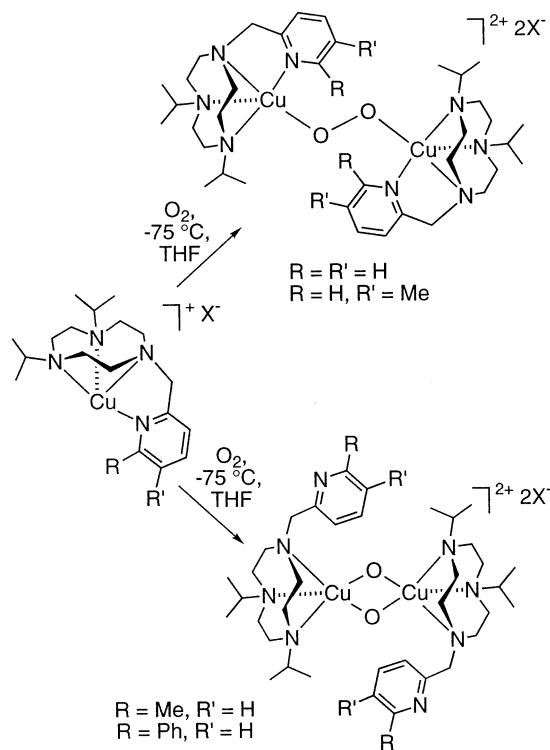


Fig. 6. Cationic portion of the X-ray crystal structure of $[L^P Cu(\text{ONO})]O_3\text{SCF}_3 \cdot \text{CH}_2\text{Cl}_2$ showing non-hydrogen atoms as 50% ellipsoids.

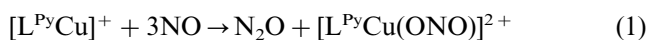


Scheme 3.

bound by all donors of the L^{Py} ligand and a single O atom of the nitrite ion in a square pyramidal geometry ($\tau = 0.003$) with an amine N atom (N7) occupying the axial coordination site (Cu1–N7 = 2.292(2) Å). Nitrite ion bond alternation ($\Delta(N-O) = 0.078$ Å) and a long Cu1...O2 distance (2.779 Å) offer convincing evidence of weak or non-existent Cu1–O2 bonding. The Cu–O_{nitrite} bond length (1.982(2) Å) is only slightly longer than the Cu(I)–O_{nitrite} bond length observed in the dicopper(I)–nitrite complex $\{[(iPr_3TACN)Cu]_2(\mu-NO_2)\}PF_6$ (1.968(2) Å) [24] and in $[(TPMA)Cu(NO_2)]PF_6$ (1.938(2) Å) [33] wherein the nitrite O atom occupies an axial position in the trigonal-bipyramidal complex ($\tau = 0.74$). These Cu–O_{nitrite} bond lengths are uniformly shorter than those observed in the (η^2-O,O) -nitrite complexes $[(Ph_3P)_2Cu(NO_2)]$ (2.191(4) Å) [34], $\{[(iPr_3TACN)Cu]_2(\mu-NO_2)\}[B(Ar)_4]_2$ (2.047(9) and 2.13(1) Å) [24], and $Tp^{Me_2}Cu(NO_2)$ [18b].

The observed products of the reaction of NO with $[L^{Py}Cu]^+$ are indicative of a NO reductive disproportionation reaction (Eq. (1)) similar to that observed with tris(pyrazolyl)hydroborate-copper(I) complexes [18]. In the reactions of NO with these latter complexes mononuclear copper–nitrosyl complexes were identified. However, no spectroscopically identifiable intermediates were observed upon treatment of solutions $[L^{Py}Cu]CF_3SO_3$ with NO either at 25 or $-78^\circ C$. The NO reactivity we observed differs significantly from that seen with complexes of TPA [17] or R_3TACN [19] (Fig. 1). It is thus

apparent that small changes in ligand denticity (tri- vs. tetradentate) and/or ligand type (aromatic vs. aliphatic N-donor) can dramatically alter the pathway of a Cu(I)/NO reaction.



3.4.3. Dioxygen

The course of low temperature oxygenations of the copper(I) complexes depends on the nature of the heterocyclic appendage (Scheme 3). Oxygenation of cold (ca. $-75^\circ C$) yellow solutions of $[L^{Py}Cu]O_3SCF_3$ or $[L^{5MePy}Cu]SbF_6$ in THF results in an immediate color change to deep purple. UV–Vis and resonance Raman spectroscopic data obtained for these solutions are similar to those of the fully characterized *trans*-1,2-peroxo complex $[(TPMA)_2Cu_2(O_2)]^{2+}$ [10] (Table 1). Thus, the purple species exhibit diagnostic CT absorption bands and resonance enhanced ($\lambda_{ex} = 572$ nm) ^{18}O -sensitive features in the Raman spectrum attributable to peroxide O–O and Cu–O vibrations (Fig. S3 in Supplementary material). The purple solutions are EPR silent, indicative of strong antiferromagnetic coupling between the Cu(II) ions. On the basis of the combined data, we formulate the oxygenation products as *trans*-1,2-peroxodicopper complexes $[(L^P Cu)_2(O_2)](X)_2$ ($P = Py$, $X = O_3SCF_3$; $P = 5MePy$, $X = SbF_6$) analogous to the TPA-supported species.

Instead of generating a purple solution upon low temperature oxygenation, $[L^{6PhPy}Cu]SbF_6$ in THF reacts with O_2 to produce intense yellow solutions at concentrations suitable for UV–Vis spectroscopic analysis (~ 1 mM) and orange–brown solutions at higher concentrations (~ 10 mM). Spectroscopic data (Table 1) indicate that the oxygenated product in this case is a bis(μ -oxo)dicopper species $[(\eta^3-L^{6PhPy}Cu)_2(\mu-O)_2](SbF_6)_2$ (Scheme 3). Particularly diagnostic spectral features similar to those identified previously for the bis(μ -oxo)dicopper unit (e.g. for the complex of Bn_3TACN as shown in Table 1) are the intense CT absorptions, resonance enhanced ($\lambda_{ex} = 457$ nm) ^{18}O -sensitive $[Cu_2(\mu-O)_2]^{2+}$ core vibrations in the Raman spectrum, and EPR silence. Further characterization of $[(L^{6PhPy}Cu)_2(\mu-O)_2](SbF_6)_2$ by techniques such as mass spectrometry or manometry was precluded due to the rapid rate of decomposition of the complex at about $-75^\circ C$ (vide infra). Due to the similarities of the spectral properties to simple R_3TACN derivatives, we hypothesize that formation of the bis(μ -oxo)dicopper complex supported by the L^{6PhPy} ligand is accompanied by loss of coordination of the pyridyl group. Thus, the different fates of the Cu(I) complexes of L^{Py} and L^{5MePy} versus that of L^{6PhPy} upon oxygenation are directly related to the coordination of the heterocyclic appendage. In the L^{Py} and L^{5MePy} cases the pyridyl unit remains coordinated, favoring

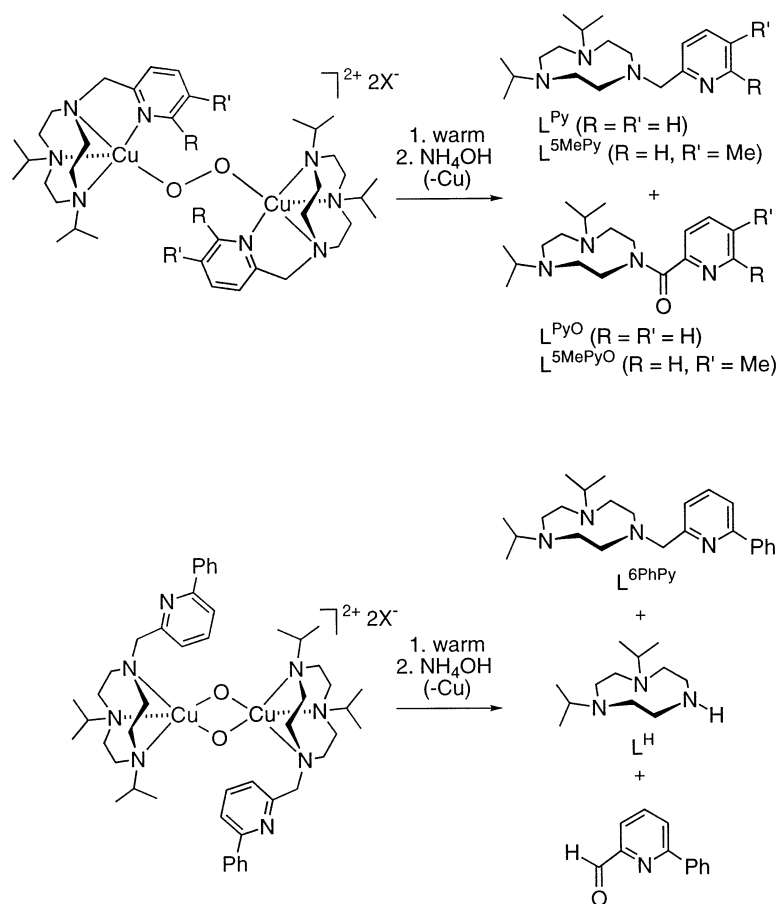
trans-1,2-peroxy generation, whereas pyridyl dissociation facilitated by the sterically bulky 6-phenyl group on $L^{6\text{PhPy}}$ yields a $[\eta^3\text{-}L^{6\text{PhPy}}\text{Cu}]^+$ fragment amenable to bis(μ -oxo) core formation. Note that the steric features associated with the $[\eta^3\text{-}L^{6\text{PhPy}}\text{Cu}]^+$ fragment are very similar to $[\text{L}^{\text{iPr}2\text{Bn}}\text{Cu}]^+$, which also yields a bis(μ -oxo)dicopper core (rather than a (μ - η^2 : η^2 -peroxy)dicopper isomer) upon oxygenation [32].

The results of the oxygenations of THF solutions of $[\text{L}^{6\text{MePy}}\text{Cu}]\text{SbF}_6$ and $[\text{L}^{\text{Quin}}\text{Cu}]\text{SbF}_6$ are less clear than those described above. In the case of $[\text{L}^{6\text{MePy}}\text{Cu}]\text{SbF}_6$, treatment with O_2 at -75°C caused an increase in the intensity of the yellow color of the solution followed by bleaching to a pale green solution. UV–Vis spectroscopic monitoring of the oxygenation process (~ 5 min, mild O_2 bubble) revealed the formation of a new feature at 430 nm that grew in and then rapidly decayed. During this process, the MLCT band of the Cu(I) complex (364 nm) gradually diminished, but the spectra obtained were always indicative of the presence of both the Cu(I) complex and the initial oxygenated product. We speculate that a bis(μ -oxo)dicopper core akin to that seen for the $L^{6\text{PhPy}}$ case forms, again due to pyridyl arm loss facilitated by the steric hindrance of the 6-substituent, but in this instance it is more reactive (vide

infra), perhaps due to less steric protection by the 6-methyl versus the 6-phenyl group. Finally, treatment of a THF solution of $[\text{L}^{\text{Quin}}\text{Cu}]\text{SbF}_6$ with dioxygen at about -75°C resulted in a bleaching of the orange color of the Cu(I) complex over the course of ~ 1 – 2 min with formation of a pale green solution as the final product. This bleaching corresponds to the loss of the 416 nm MLCT band of $[\text{L}^{\text{Quin}}\text{Cu}]\text{SbF}_6$. Careful monitoring of the oxygenation process (mild bubbling) at about -75°C , scanning every ~ 10 s, did not reveal the formation of any spectroscopically identifiable copper–dioxygen species.

Both types of dioxygen adducts described above, the *trans*-1,2-peroxy and bis(μ -oxo)dicopper complexes, decompose upon warming, but via different pathways. We reported previously that warming of solutions of $[(\text{L}^{\text{Py}}\text{Cu})_2(\text{O}_2)](\text{O}_3\text{SCF}_3)_2$ followed by extraction of the copper ions with NH_4OH yielded a mixture of L^{Py} and a new modified ligand L^{PyO} in a 4:1 ratio ($\sim 75\%$ total recovery) (Scheme 4) [22]. We also have found that the analogous compound $[(\text{L}^{5\text{MePy}}\text{Cu})_2(\text{O}_2)](\text{SbF}_6)_2$ exhibits similar reactivity upon decomposition, yielding $L^{5\text{MePy}}$ and $L^{5\text{MePyO}}$ in a $\sim 2:1$ ratio ($\sim 61\%$ total recovery).

In contrast to the ligand oxygenation resulting from decay of the *trans*-1,2-peroxy complexes, decompos-



Scheme 4.

ition of the bis(μ -oxo)dicopper complex $[(L^{6PhPy}Cu)_2(\mu-O)_2](SbF_6)_2$ results in oxidative N-dealkylation of the heterocyclic appendage. Thus, warming of solutions of $[(L^{6PhPy}Cu)_2(\mu-O)_2](SbF_6)_2$ followed by removal of the copper ions from the green solution by treatment with NH_4OH resulted in the isolation of a 3:2 mixture of L^{6PhPy} and L^H and a trace amount of 6-phenyl-2-pyridinecarboxaldehyde ($\sim 87\%$ total recovery). This type of N-dealkylation reactivity was shown previously [35] to be the predominant pathway of decomposition of bis(μ -oxo)dicopper complexes. However, the observation of N-dealkylation at the pseudobenzyl position of the ligand contrasts with the isopropyl substituent cleavage seen upon decomposition of $\{[(^iPr_2BnTACN)Cu]_2(\mu-O)_2\}(ClO_4)_2$. The differences observed in the regioselectivity of these N-dealkylation reactions may indicate that additional factors associated with the 6PhPy substituent may influence the observed oxidative chemistry.

Although copper–dioxygen species could not be conclusively identified in low-temperature oxygenation reactions of either $[L^{6MePy}Cu]SbF_6$ or $[L^{Quin}Cu]SbF_6$, similar ligand product ratios to those observed for the decomposition of $[(L^{6PhPy}Cu)_2(\mu-O)_2](SbF_6)_2$ ($\sim 3:2 L^P:L^H$, $> 85\%$ total recovery; $P = 6MePy$, $Quin$) were obtained. Therefore, we propose that the L^{6PhPy} , L^{6MePy} , and L^{Quin} systems all proceed through bis(μ -oxo)dicopper intermediate complexes which decompose via a C–H activation process at the pyridyl- or quinolyl-methyl position of the heterocyclic appendage. Our inability to observe and/or characterize the intermediate bis(μ -oxo)dicopper complexes in the L^{6MePy} and L^{Quin} systems suggests that the thermal stability of this family of complexes is highly dependent upon the nature of the heterocyclic appendage, an effect that at present we do not understand.

4. Summary and conclusions

A series of Cu(I) complexes of hybrid ligands comprising 1,4-diisopropyl-1,4,7-triazacyclononane appended to variably substituted pyridyl or quinolyl donors have been characterized and their reactions with CO, NO, and O_2 explored. With CO, displacement of the heterocyclic arm occurs reversibly to yield adducts with the ligand coordinated only through its macrocyclic N donor atoms in η^3 fashion. Disproportionation of NO is promoted by the Cu(I) complex of L^{Py} , yielding N_2O and a Cu(II)– NO_2^- complex in which the nitrite is η^1 -O-bound and L^{Py} is coordinated η^4 . The reactions with O_2 vary according to the specific heterocyclic appendage, with steric effects of the heterocyclic substituents being of paramount importance. Thus, the pyridyl unit remains bound to the metal in the less hindered cases (L^{Py} and L^{5MePy}) to yield *trans*-1,2-per-

oxo complexes, but when the 6-substituents are present the heterocycle is ejected and bis(μ -oxo)dicopper complex formation is observed (L^{6PhPy}) or implicated (L^{Quin} and L^{6MePy}). The *trans*-1,2-peroxo and bis(μ -oxo) species decompose differently to yield ligands that are either oxygenated or N-dealkylated, respectively. These results imply different pathways for the decay of the structurally divergent species, but also may be explained by invoking similar initial steps for the oxygenated complexes (e.g. attack at ligand methylene C–H bond to yield an –OH group) but a different fate for the subsequent intermediate (ketone formation vs. N-dealkylation) due to inherent differences in the reactivity of the ligands.

When compared to the ligands portrayed in Fig. 1, the hybrid ligands described herein display behavior in their copper(I)-small molecule chemistry that is intermediate between that seen when R_3TACN and $TMPA$ are used. This behavior for the L^P ligands can be traced to their ability to adopt η^4 or η^3 coordination geometries, which is, in turn, subject to the steric influences of the heterocyclic ring substituents. Thus, our studies show that ligand substituent size and shape are significant determinants of the reactivity of Cu(I) compounds with CO, NO, and O_2 and provide further support for the notion that such steric effects are of general importance in metallobiochemistry and catalysis.

5. Supplementary material

VT 1H NMR data for $[L^{Py}Cu]SbF_6$ (Fig. S1), UV–Vis data for the reversible binding of CO to $[L^{Py}Cu]SbF_6$ (Fig. S2), resonance Raman spectra for the *trans*-peroxo complexes supported by L^{Py} and L^{5MePy} (Fig. S3), and full reports of X-ray crystallographic data (22 pages).

Acknowledgements

We thank the National Institutes of Health (GM47365 to W.B.T. and a postdoctoral fellowship to L.M.B.), the National Science Foundation (National Young Investigator Award to W.B.T.), and the Alfred P. Sloan and Camille & Henry Dreyfus Foundations for financial support. We also thank Dr Carole Toia for assistance.

References

- [1] Selected lead references: (a) A.L. Feig, S.J. Lippard, Chem. Rev. 94 (1994) 759. (b) B.J. Wallar, J.D. Lipscomb, Chem. Rev. 96 (1996) 2625. (c) L. Que Jr., R.Y.N. Ho, Chem. Rev. 96 (1996) 2607. (d) E.I. Solomon, U.M. Sundaram, T.E. Machonkin, Chem. Rev. 96 (1996) 2563. (g) J.P. Klinman, Chem. Rev. 96 (1996) 2541.

- [2] S. Moncada, J. Stamler, S. Gross, E.A. Higgs, (Eds.), *The Biology of Nitric Oxide*, Part 5, Portland Press, London, 1996.
- [3] See for example: (a) V.I. Chen, A.M. Orville, M.R. Harpel, C.A. Frolik, K.K. Surerus, E. Münck, J.D. Libscomb, *J. Biol. Chem.* 264 (1989) 21677. (b) B.J. Reedy, N.J. Blackburn, *J. Am. Chem. Soc.* 116 (1994) 1924.
- [4] K.D. Karlin, *Science* 261 (1993) 701.
- [5] Reviews: (a) K.D. Karlin, S. Kaderli, A.D. Zuberbühler, *Acc. Chem. Res.* (1997) 139. (b) W.B. Tolman, *Acc. Chem. Res.* 30 (1997) 227. (c) S. Fox, K.D. Karlin, in: J.S. Valentine, C.S. Foote, A. Greenberg, J.F. Liebman (Eds.), *Active Oxygen in Biochemistry*, Blackie Academic & Professional, Chapman & Hall, Glasgow, Scotland, 1995. (d) N. Kitajima, Y. Moro-oka, *Chem. Rev.* 94 (1994) 737. (e) K.D. Karlin, Z. Tyeklár, A.D. Zuberbühler, in: J. Reedijk (Ed.), *Bioinorganic Catalysis*, Marcel Dekker, New York, 1993. (f) T.N. Sorrell, *Tetrahedron* 40 (1989) 3. (g) K.D. Karlin, Y. Gultneh, *Prog. Inorg. Chem.* 35 (1987) 219. (h) W.B. Tolman, in: H.H. Thorp (Ed.), *Synthetic Modeling of the Interactions of Nitrogen Oxides with Copper Proteins*, vol. 7, American Chemical Society, Washington, 1995.
- [6] (a) K.D. Karlin, J.C. Hayes, J. Shi, J.P. Hutchinson, J. Zubieta, *Inorg. Chem.* 21 (1982) 4106. (b) J. Zubieta, K.D. Karlin, J.C. Hayes, in: K.D. Karlin, J. Zubieta (Eds.), *Copper Coordination Chemistry: Biochemical and Inorganic Perspectives*, Adenine Press, New York, 1983. (c) G. Anderegg, F. Wenk, *Helv. Chim. Acta* 50 (1967) 2330.
- [7] (a) S. Trofimenko, *Chem. Rev.* 93 (1993) 943. (b) G. Parkin, *Adv. Inorg. Chem.* 42 (1995) 291. (c) N. Kitajima, W.B. Tolman, *Prog. Inorg. Chem.* 43 (1995) 419.
- [8] K. Wieghardt, P. Chaudhury, *Prog. Inorg. Chem.* 35 (1988) 329.
- [9] (a) T.N. Sorrell, W.E. Allen, P.S. White, *Inorg. Chem.* 34 (1995) 952. (b) W.E. Allen, T.N. Sorrell, *Inorg. Chem.* 36 (1997) 1732. (c) W.E. Lynch, J.D.M. Kurtz, S. Wang, R.A. Scott, *J. Am. Chem. Soc.* 116 (1994) 11030. (d) I. Sanyal, M. Mahroof-Tahir, M.S. Nasir, P. Ghosh, B.I. Cohen, Y. Gultneh, R.W. Cruse, A. Farooq, K.D. Karlin, S. Liu, J. Zubieta, *Inorg. Chem.* 31 (1992) 4322. (e) S. Itoh, H. Nakao, L.M. Berreau, T. Kondo, M. Komatsu, S. Fukuzumi, *J. Am. Chem. Soc.* 120 (1998) 2890. (f) H.V. Obias, Y. Lin, N.N. Murthy, E. Pidcock, E.I. Solomon, M. Ralle, N.J. Blackburn, Y.M. Neubold, A.D. Zuberbühler, K.D. Karlin, *J. Am. Chem. Soc.* 120 (1998) 12960. (g) T.N. Sorrell, D.L. Jameson, *Inorg. Chem.* 21 (1982) 1014. (h) V. Mahadevan, Z. Hou, A.P. Cole, D.E. Root, T.K. Lal, E.I. Solomon, T.D.P. Stack, *J. Am. Chem. Soc.* 119 (1997) 11996. (i) A.P. Cole, D.E. Root, P. Mukherjee, E.I. Solomon, T.D.P. Stack, *Science* 273 (1996) 1848. (j) J.S. Thompson, *J. Am. Chem. Soc.* 106 (1984) 8308.
- [10] Z. Tyeklár, R.R. Jacobson, N. Wei, N.N. Murthy, J. Zubieta, K.D. Karlin, *J. Am. Chem. Soc.* 115 (1993) 2677.
- [11] K.D. Karlin, N. Wei, B. Jung, S. Kaderli, A.D. Zuberbühler, *J. Am. Chem. Soc.* 113 (1991) 5868.
- [12] N. Wei, N.N. Murthy, Q. Chen, J. Zubieta, K.D. Karlin, *Inorg. Chem.* 33 (1994) 1953.
- [13] (a) M. Harata, K. Jitsukawa, H. Masuda, H. Einaga, *J. Am. Chem. Soc.* 116 (1994) 10817. (b) L.M. Berreau, S. Mahapatra, J.A. Halfen, V.G. Young Jr., W.B. Tolman, *Inorg. Chem.* 35 (1996) 6339. (c) M. Harata, K. Jitsukawa, H. Masuda, H. Einaga, *Bull. Chem. Soc. Jpn* 71 (1998) 637.
- [14] N. Kitajima, K. Fujisawa, C. Fujimoto, Y. Moro-oka, S. Hashimoto, T. Kitagawa, K. Toriumi, K. Tatsumi, A. Nakamura, *J. Am. Chem. Soc.* 114 (1992) 1277.
- [15] (a) K.A. Magnus, B. Hazes, H. Ton-That, C. Bonaventura, J. Bonaventura, W.G.J. Hol, *Proteins* 19 (1994) 302. (b) K.A. Magnus, H. Ton-That, J.E. Carpenter, *Chem. Rev.* 94 (1994) 727. (c) E.I. Solomon, F. Tucek, D.E. Root, C.A. Brown, *Chem. Rev.* 94 (1994) 827. (d) C. Eiken, F. Zippel, K. Büldt-Karentzpoulos, B. Krebs, *FEBS Lett.* 436 (1998) 293.
- [16] K. Fujisawa, M. Tanaka, Y. Moro-oka, N. Kitajima, *J. Am. Chem. Soc.* 116 (1994) 12079.
- [17] P.P. Paul, K.D. Karlin, *J. Am. Chem. Soc.* 113 (1991) 6331.
- [18] (a) C.E. Ruggiero, S.M. Carrier, W.E. Antholine, J.W. Whittaker, C.J. Cramer, W.B. Tolman, *J. Am. Chem. Soc.* 115 (1993) 11285. (b) C.E. Ruggiero, S.M. Carrier, W.B. Tolman, *Angew. Chem., Int. Ed. Engl.* 33 (1993) 895. (c) J.L. Schneider, S.M. Carrier, C.E. Ruggiero, V.G. Young Jr., W.B. Tolman, *J. Am. Chem. Soc.* 120 (1998) 11408.
- [19] S. Mahapatra, J.A. Halfen, W.B. Tolman, *J. Chem. Soc., Chem. Commun.* (1994) 1625.
- [20] A pertinent example: M.S. Nasir, R.R. Jacobson, J. Zubieta, K.D. Karlin, *Inorg. Chim. Acta* 203 (1993) 5.
- [21] K.P. Wainwright, *Coord. Chem. Rev.* 166 (1997) 35.
- [22] (a) J.A. Halfen, V.G. Young Jr., W.B. Tolman, *J. Am. Chem. Soc.* 118 (1996) 10920. (b) J.A. Halfen, Ph.D. Thesis, University of Minnesota, 1996.
- [23] J.A. Halfen, W.B. Tolman, *Inorg. Synth.* 34 (1998) 75.
- [24] J.A. Halfen, S. Mahapatra, E.C. Wilkinson, A.J. Gengenbach, V.G. Young Jr., L. Que Jr., W.B. Tolman, *J. Am. Chem. Soc.* 118 (1996) 763.
- [25] A. Furstner, A. Ernst, *Tetrahedron* 51 (1995) 773.
- [26] A. Nanthakumar, S. Fox, N.N. Murthy, K.D. Karlin, *J. Am. Chem. Soc.* 119 (1997) 3898.
- [27] C. Chuang, K. Lim, Q. Chen, J. Zubieta, J.W. Canary, *Inorg. Chem.* 34 (1995) 2562.
- [28] G.J. Kubas, *Inorg. Synth.* 19 (1979) 90.
- [29] SHELXTL-PLUS Version 5.0, Siemens Industrial Automation, Madison, WI.
- [30] M. Melnik, L. Macaskova, C.E. Holloway, *Coord. Chem. Rev.* 126 (1993) 71.
- [31] D.D. Perrin, *Dissociation Constants of Organic Bases in Aqueous Solutions*, Supplement 1972, Butterworth, London, 1972.
- [32] S. Mahapatra, J.A. Halfen, E.C. Wilkinson, G. Pan, X. Wang, V.G. Young Jr., C.J. Cramer, L. Que Jr., W.B. Tolman, *J. Am. Chem. Soc.* 118 (1996) 11555.
- [33] N. Komeda, H. Nagao, Y. Kushi, G. Adachi, M. Suzuki, A. Uehara, K. Tanaka, *Bull. Chem. Soc. Jpn.* 68 (1995) 581.
- [34] J.A. Halfen, W.B. Tolman, *Acta Crystallogr., Sect. C* 51 (1995) 215.
- [35] S. Mahapatra, J.A. Halfen, W.B. Tolman, *J. Am. Chem. Soc.* 118 (1996) 11575.